Reactive power potential of converter-connected renewables using convex power flow optimization

Baviskar, Aeishwarya; Hansen, Anca D.; Das, Kaushik; Ul Nazir, Firdous

Published in:
International Journal of Electrical Power and Energy Systems

Link to article, DOI:
10.1016/j.ijepes.2023.109193

Publication date:
2023

Document Version
Publisher's PDF, also known as Version of record

Electrical Power and Energy Systems 152 (2023) 109193

Contents lists available at ScienceDirect

International Journal of Electrical Power and Energy Systems

journal homepage: www.elsevier.com/locate/ijepes

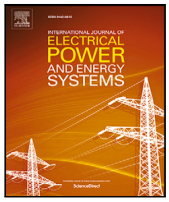

Reactive power potential of converter-connected renewables using convex power flow optimization

Aeishwarya Baviskar [a,*], Anca D. Hansen [a], Kaushik Das [a], Firdous Ul Nazir [b]

[a] Department of Wind and Energy Systems, Technical University of Denmark, Risø Campus, Roskilde, 4000, Denmark
[b] Department of Electrical and Electronic Engineering, Glasgow Caledonian University, Cowcaddens Road, Glasgow, G4 0BA, United Kingdom

ARTICLE INFO

Keywords:
Converter-connected RES
Reactive power capability
Grid code requirements
Convex optimization
Loss minimization
Wind power plants

ABSTRACT

Converter-connected renewable energy sources (RES) in the distribution network alter the power flow in the network. Often, grid reinforcements and additional local reactive power sources are needed to maintain steady state network operation. Converter-connected RES is an accessible local reactive power source for distribution system operators to optimize network operations. However, the non-linearity and non-convexity in the converter equations make their modelling challenging, which further results in the under-utilization of the reactive power capability from these sources. Oftentimes, the converter-connected generator is partially modelled using only apparent power constraints. This paper presents an approach based on Schur's complement and piecewise planar approximation to incorporate the converter equations in a convex power flow optimization routine. The advantages of employing complete converter capabilities for optimal operation of the distribution network are studied via simulations on a real distribution network dataset. A comparison between deploying reactive power according to the minimum grid codes requirement, partial modelling of the converter, and complete converter capabilities is correspondingly presented. Active power losses decrease by 4.1% over 10 month period with high penetration of renewable generation. Furthermore, the voltage profile in the distribution network is improved and the reactive power dependency on the transmission network is reduced.

1. Introduction

Power systems worldwide stand on the frontier of a transition by viable interest in distributed energy sources and the desire to accommodate increasing amounts of renewable energy sources (RES) into the energy mix. Amongst all, distribution system operators (DSO) find themselves on a unique platform to integrate prosumers who wish to deliver excess power to the grid but depend on it for a reliable and secure power connection. These competing interests have become a major challenge for the DSOs [1].

Past trends, data, and renewable energy targets around the globe have been hinting at the changing landscape of power generation in the future. About 510 GW of renewable capacity is expected to be added to the power system in Europe by the year 2030, approximately 70% of which is predicted to be connected to the distribution network [2]. Approximately 50% of the total new RES, in economies like Germany, France, Italy, and Portugal, will be connected to the distribution grid. Similarly, to fulfil the renewable energy targets, India also marks an uptake of approximately 40 GW of rooftop solar by 2022 [3]. In addition to the major RES sources like solar and wind energy, electric vehicles (EV) and EV fast charging stations are also predicted to have a stellar rise in the distribution network [2].

The current distribution network is not well equipped to face extensive challenges due to upcoming distributed energy sources like wind power plants, and photovoltaic and EV systems. The shortcomings in the infrastructure, hosting capacity, and, operation of the distribution networks become relevant, underlining the requirement for reinforcements, grid modernization, and flexible energy sources [4–8]. Barring the challenges and disadvantages, advanced control capabilities of the converters accompanying RES can be utilized to support DSO. Depending on resource availability, the converters connecting the RES to the grid generally operate below their maximum rated power. Thus, the converters can be used as a flexible local reactive power source in the distribution network.

European grid codes have adapted over time, recognizing the control capabilities of converter-connected RES. European Commission Regulations (with Danish Specifications), for example, require RES to provide certain reactive power capabilities depending on their installed capacity [9,10]. The FERC Order 2222 in the USA also moves towards incorporating flexible resources from distributed generation

* Corresponding author.
E-mail address: aeish@dtu.dk (A. Baviskar).

https://doi.org/10.1016/j.ijepes.2023.109193
Received 19 September 2022; Received in revised form 13 January 2023; Accepted 19 April 2023

sources [11]. Nevertheless, the big potential of converter-connected RES to provide reactive power remains under-utilized in the grid codes as they restrict the reactive power within a proportion of the total power rating or with a pre-defined power factor.

The reactive power potential from converter-connected RES is utilized for applications not limited to voltage control but other network applications like hosting capacity analysis, reactive power control, optimal operation of distribution networks, and exploration of reactive power markets in the future grid. Yet several research works restrict the reactive power from RES within a certain power factor range [12–20]. Grid codes are also often used to define the constraints on reactive power from RES [21–23]. The power factor and minimum specified grid codes are limiting constraints and do not capture the reactive power potential of the converter-connected RES.

Another approach to model the reactive power from RES is to use the apparent power limits or the rated current limit defined below.

$$Q_{RES} \leq \sqrt{S_{max}^2 - P_{RES}^2}$$

where Q_{RES} is the reactive power from RES, P_{RES} is the active power generated, and S_{max} is the installed apparent power. To account for the maximum rated current for the converter, S_{max} can be replaced by the term $|V_{pc} I_{max}|$, where V_{pc} is the voltage at the point of connection and I_{max} is the maximum current rating. The reactive power potential of a converter depends on two factors; the rated current I_{max} and, the minimum and maximum rated voltage for the converter. Most research works focus on the maximum current constraint on the converters and fail to account for the converter voltage constraints, thus leaving the converter reactive power capability model incomplete [13,16,24–35]. Quite often this results in an overestimation of the reactive power capabilities of the power electronic converter at critical timestamps. The network operator subsequently runs into the risk of huge penalties and/or unnecessary investment expenditure as a result of such overestimation and/or underutilization of the RES reactive power potential. Thus, a complete converter model including not only the rated current but also converter voltage limits has to be considered.

The fully rated converter-connected RES model with current and minimum and maximum voltage limits are developed in [36–40]. A complete doubly fed induction generator model is used in [41] to account for the reactive power from a wind power plant (WPP), while [42] uses models of the converter with maximum current and maximum voltage limits only. More recently, authors in [40] propose to enhance the reactive power potential of a WPP using the complete converter constraint model as suggested in [36–38]. However, a linearization approach for the constraints based on Taylor series expansion is used for all the reactive power constraints of the WPP.

Two research gaps are identified from the available literature. The first one concerns the accurate modelling of the reactive power potential from RES as a local reactive power source. The research so far either under-utilizes or overestimates the available reactive power capacity from RES. To the author's knowledge, quantifying the overestimation or under-utilization of the reactive power capability from RES has not surfaced in the literature. The authors hypothesize that the under-utilization of reactive power from RES through grid codes and overestimation through partial modelling using only apparent power constraints leads to significant errors in system operation, especially in studies that focus on utilizing RES reactive power capability to avoid grid reinforcements or enable a more active distribution grid role in reactive power markets. Thus, inaccurate and insufficient quantification of the available reactive power potential can be detrimental. This research quantifies the underutilized and overestimated reactive power capability from converter-connected RES.

The second research gap is to include the complete reactive power model for converter-connected RES in a convex power flow framework, guaranteeing extensive utilization of the reactive power from the available converter-connected resources. This article develops a novel methodology to incorporate the current and voltage constraints in optimal power flow using a convex power flow optimization for the first time. The results from simulations conducted over 10 months on a real Danish distribution network validate the value of the developed methodology. The validation is performed by overestimation/under-utilization of the available reactive power capabilities from RES obtained from partially modelling the converter system (as in current literature) compared to the proposed methodology.

It should be highlighted that the typical power flow model is non-linear and non-convex, thus the power flow optimization problem becomes a non-deterministic polynomial time (NP) hard problem to solve. In addition to the non-linearity and non-convexity already existing in the power flow model, the converter model accompanying RES contributes with supplementary non-linearity to the already NP-hard optimization problem. Meta-heuristic approaches are typically adopted to solve the power flow optimization by most research studies [12,27,43–45]. However, such methods lack the guarantee for a globally optimal solution. Two other popular methods existing in literature to solve the problem of optimizing active distribution network operation are analytical, as pointed out in [30,32,44], or based on linearization of the power flow equations and/or converter constraints, as demonstrated by [19,40,46].

To solve this NP-hard problem, a conic quadratic formulation is introduced in [47] in an attempt to convexify the optimization. Research works using a semidefinite programming (SDP) relaxation for solving optimal power flow have proven to be quite influential due to the guarantee of a global optimum [48–52]. This approach has been further extended to reactive power optimization, state estimation, security-constrained optimal power flow, and multi-objective formulations in distribution networks, to name a few [20,24,53–56]. The SDP model solves this research's power flow optimization problem as it guarantees a global minimum for the relaxed convex problem, provided the rank conditions are satisfied. Thus, the maximum benefit of reactive power from RES with a complete converter constraint model can be demonstrated.

The research presented in this article aims, therefore, to fill the gap in the existing literature with the following contributions:

1. Incorporation of non-linear converter equations into a convex power flow optimization framework, namely considering the modelling of non-linear, non-convex converter constraints inside the convex SDP formulation to find global optima while keeping the resultant optimizer convex.
2. Quantification of the under-utilization of reactive power from RES with respect to grid codes and overestimation of the reactive power potential by modelling the converter with only apparent power/rated current constraint in absolute terms, i.e. via calculating the feasible reactive power area.
3. Comparative analysis of reactive power from RES to minimize active power losses in a distribution network amongst the following scenarios,
    - Minimum specified grid code requirements as converter constraints (under-utilization)
    - Only maximum current constraint (overestimation)
    - Complete converter model with current, minimum, and maximum voltage constraints

The power flow optimization is implemented in this research on a real distribution grid model with load and generation time series for about a year to demonstrate the benefits of exploiting converter-connected generators' exhaustive reactive power capability. The results from this research indicate the potential maximum benefits for the distribution network in terms of reduction in active power loss, voltage profile improvement, and reduced dependence on the transmission network for reactive power supply.

The article is organized as follows. Section 2 briefly introduces the convex SDP optimization and details the modelling of non-convex converter equations. The data for the distribution grid and case studies are

elaborated in Section 3, whereas the results from the comparative case study are presented and discussed in Section 4. Section 5 concludes the paper by emphasizing relevant results and learning from the research.

2. Optimization problem formulation

This section introduces the classical loss minimization problem in a distribution network with converter-connected RES. SDP model is used for the optimization. Additionally, convex formulations and approximations for the converter constraints are introduced.

2.1. Classical loss minimization problem

Let $\mathcal{N}$ be the set of all the buses in the network and $(l,m) \in \mathcal{L}$ be the set of distribution lines connecting buses l and $m \in \mathcal{N}$. Let $\mathcal{G}$ be the set of buses with converter-connected generations, such that $\mathcal{G} \subseteq \mathcal{N}$. The active and reactive power demand at bus k for a particular time instance is denoted by P_{D_k} and Q_{D_k}, respectively. Whereas the active and reactive power generation at bus k is denoted by P_{G_k} and Q_{G_k} for $k \in \mathcal{G}$ respectively. Note that the generator sign convention is used in this research, which means that negative values indicate a power demand and positive values indicate power generation. Respective values of P_{lm} and $\overline{S}_{lm}$ stand for the active and apparent power (complex variable) in the distribution line $(l,m) \in \mathcal{L}$, while the complex voltage at bus k is $\overline{V}_k$.

Power flow in a distribution grid is subject to constraints on active and reactive power injection at each bus denoted by P_k and Q_k, apparent power flow through the distribution lines, and voltage at each bus.

$$P_k = P_{G_k} - P_{D_k} \qquad \forall k \in \mathcal{N} \tag{1a}$$

$$Q_k = Q_{G_k} - Q_{D_k} \qquad \forall k \in \mathcal{N} \tag{1b}$$

$$P_{G_k}^{min} \le P_{G_k} \le P_{G_k}^{max} \qquad \forall k \in \mathcal{G} \tag{1c}$$

$$Q_{G_k}^{min} \le Q_{G_k} \le Q_{G_k}^{max} \qquad \forall k \in \mathcal{G} \tag{1d}$$

$$V_k^{min} \le |\overline{V}_k| \le V_k^{max} \qquad \forall k \in \mathcal{N} \tag{1e}$$

$$|\overline{S}_{lm}| \le S_{lm}^{max} \qquad \forall (l,m) \in \mathcal{L} \tag{1f}$$

$$|P_{lm}| \le P_{lm}^{max} \qquad \forall (l,m) \in \mathcal{L} \tag{1g}$$

where, $P_{G_k}^{min}, Q_{G_k}^{min}, P_{G_k}^{max}, Q_{G_k}^{max}$ $\forall k \in \mathcal{G}$ are the minimum and maximum active and reactive power limits for generators at bus $k \in \mathcal{G}$. For buses without any generating source P_{G_k} and Q_{G_k} in (1a) and (1b) are zero. V_k^{min} and V_k^{max} are the minimum and maximum bounds on the bus voltage magnitude, and S_{lm}^{max} is the apparent power flow rating for the distribution line $(l,m) \in \mathcal{L}$.

The objective of active power loss minimization is the sum of the total active generation subtracted by the total active power demand/consumption at all buses in the network as follows,

$$\min_{\overline{V}_k} \sum_{k \in \mathcal{N}} (P_{G_k} - P_{D_k}) \tag{2}$$

A classical loss minimizing optimization is formulated with the objective, (2) subject to distribution grid constraints given in (1c), (1e), (1f), (1g), and the converter constraints. Some constraints mentioned may not be of utmost relevance depending on specific implementations.

It should be noticed that the classical loss minimizing optimization problem is non-linear and non-convex primarily due to the interdependence and constraints between active power, reactive power, voltage magnitude, and angle. Thus, it is difficult to find a global minimum. One of the methods that come with a mathematical guarantee for tracking down the global minimum for the classical optimization problem is the SDP approach, which relaxes the non-convex problem and solves the dual of the relaxation [57].

A convex relaxation of the optimization problem is achieved by redefining the impedance matrix Y_{bus} and complex voltage vector $\mathbf{V}$ to represent the power demand at the buses, power flow in the distribution lines, and voltage magnitude. The voltage vector is re-defined as a matrix W.

$$X = [Re\{\mathbf{V}\}^T \; Im\{\mathbf{V}\}^T]^T \tag{3}$$

$$W = X X^T \tag{4}$$

Let $e_k \forall k \in \mathcal{N}$ represent a standard basis vector for the kth bus.

$$M_k = \begin{bmatrix} e_k e_k^T & 0 \\ 0 & e_k e_k^T \end{bmatrix}$$

The squared voltage magnitude at a node k can be calculated as,

$$|\mathbf{V}_k|^2 = Tr\{M_k W\}$$

where $Tr\{\}$ represents the trace of the matrix. Note that for primal SDP relaxation, W is the optimization variable. For computing the power injections the following matrices are introduced,

$$Y_k = e_k e_k^T Y_{bus} \tag{5}$$

$$\mathbf{Y_k} = \frac{1}{2} \begin{bmatrix} Re\{Y_k + Y_k^T\} & Im\{Y_k - Y_k^T\} \\ Im\{Y_k - Y_k^T\} & Re\{Y_k + Y_k^T\} \end{bmatrix} \tag{6}$$

The active power injection at any node k is computed as,

$$P_{D_k} = Tr\{\mathbf{Y}_k W\} \tag{7}$$

Similarly, the reactive power injection and active and apparent power flow through the lines are computed using the primal optimization variable W and the re-structured impedance matrices. Readers are referred to [48] for deriving the SDP relaxation.

In the above optimization, converter constraints from RES are not considered. The converter constraints further add non-linearity and non-convexity to the optimization. Thus, the constraints need to be modelled appropriately to consider RES converter capabilities to reduce the active power loss in a distribution grid, which is presented in the following section. Without the loss of generality, specific focus is given to the wind power plant (WPP) equivalent model. Regardless, the converter modelling presented in the following section can be adapted to solar PV plants. The major difference between a WPP converter model and a PV converter model is the calculation of equivalent system impedance, which is not the scope of this research work.

2.2. Converter connected RES- reactive power capability model

This section details modelling for converter-connected WPP. The converter models establish the reactive power constraints from RES.

Wind Power Plant Equivalent Model

A reactive power capability model for a WPP contains a collector system model and a converter model. Fig. 1 depicts a single wind turbine with impedance Z_{WT} connected to the grid via a collector impedance (Z_{coll}) which also includes the filter impedance and a step-up transformer. The equivalent impedance for a single wind turbine is a combination of the wind turbine impedance, collector system, filter, and transformer impedance. For a single wind turbine, Z_{G_k}, represents the impedance of the converter with the transformer, whereas for a WPP with multiple wind turbines, Z_{G_k}, represents the equivalent impedance of the collection system and the converter. The method to compute Z_{G_k} is detailed in [36,58].

A method to find an equivalent representation of a WPP collection system considering the losses in the WPP is derived in [58]. The combined equivalent WPP model with the converter model is presented in [36,42] to obtain a holistic reactive power capability model for the WPP. The detailed reactive power capability model for WPP collection system plus the converter model introduced in [36] is used in this research to embrace the reactive power capability of a WPP.

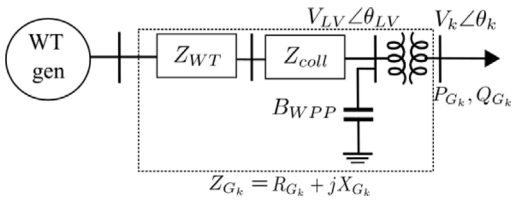

Fig. 1. Converter Connected Wind power plant model depicting a single wind turbine impedance, collector circuit, and transformer.

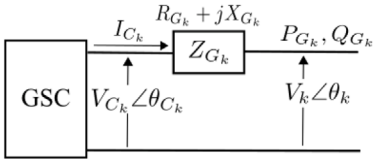

Fig. 2. Circuit diagram of a grid side converter (GSC).

Reactive Power Constraints for Converter Connected WPP

The converter system for a WPP is henceforth represented in this section by a grid side converter (GSC) with an equivalent impedance encapsulating converter, filter, and transformer impedances. Consider a simplified circuit of a GSC connected to the distribution grid, as shown in Fig. 2.

Where $V_{C_k}\angle\theta_{C_k}$ is the converter voltage magnitude and angle, respectively, I_{C_k} is the converter current, $Z_{G_k} = R_{G_k} + jX_{G_k}$ denotes the equivalent impedance of the RES system, P_{G_k}, Q_{G_k} are the active and reactive power outputs from the converter connected generation, and $V_k\angle\theta_k$ is the voltage at bus $k \in \mathcal{G}$. In the case of a PV plant, the bounds on V_{C_k} are given by the PV panel voltage V_{pv}.

The active and reactive power constraints for the GSC are as follows,

$$P_{G_k}^2 + Q_{G_k}^2 \le (V_k I_{C_k}^{max})^2 \tag{8}$$

where $I_{C_k}^{max}$ is the rated maximum converter current. The reactive power from WPPs is also a function of the voltage at bus k and converter voltage V_{C_k},

$$(P_{G_k} + \frac{V_k^2 R_{G_k}}{|Z_{G_k}|^2})^2 + (Q_{G_k} + \frac{V_k^2 X_{G_k}}{|Z_{G_k}|^2})^2 = (\frac{V_k V_{C_k}}{|Z_{G_k}|})^2$$

The reactive power is thus constrained due to the rated maximum and minimum converter voltage $V_{C_k}^{max}$ and $V_{C_k}^{min}$,

$$(P_{G_k} + \frac{V_k^2 R_{G_k}}{|Z_{G_k}|^2})^2 + (Q_{G_k} + \frac{V_k^2 X_{G_k}}{|Z_{G_k}|^2})^2 \le (\frac{V_k V_{C_k}^{max}}{|Z_{G_k}|})^2 \tag{9a}$$

$$(P_{G_k} + \frac{V_k^2 R_{G_k}}{|Z_{G_k}|^2})^2 + (Q_{G_k} + \frac{V_k^2 X_{G_k}}{|Z_{G_k}|^2})^2 \ge (\frac{V_k V_{C_k}^{min}}{|Z_{G_k}|})^2 \tag{9b}$$

The complete derivation of the active and reactive power constraints listed above can be found in [42] for WPPs and [37] for PV plants.

The voltage constraints on the converter expressed in (9) translate into upper and lower bounds on the reactive power output from the RES. The reactive power output is a quadratic function of voltage at the point of connection V_k and the active power generation from the renewable generator P_{G_k}. The constraints in (8) and (9a) are convex constraints with the feasible set as the closure of a sphere. The constraint in (9b) is non-convex with the feasible space as the outer area of a spherical surface.

Thus, converter constraints in (9b) add additional non-convexity and non-linearity to the power flow optimization. To employ an SDP approach to solve active power loss minimization problem with a large number of converter-connected generators the converter constraints from (8) and (9) need to be reformulated or relaxed as convex constraints.

(8) and (9) are re-written in terms of the SDP variables, W and M_k as follows,

$$P_{G_k}^2 + Q_{G_k}^2 \le Tr\{M_k W\}(I_{C_k}^{max})^2 \tag{10}$$

$$(P_{G_k} + \frac{Tr\{M_k W\}R_{G_k}}{|Z_{G_k}|^2})^2 + (Q_{G_k} + \frac{Tr\{M_k W\}X_{G_k}}{|Z_{G_k}|^2})^2 \le Tr\{M_k W\}(\frac{V_{C_k}^{max}}{|Z_{G_k}|})^2 \tag{11}$$

$$(P_{G_k} + \frac{Tr\{M_k W\}R_{G_k}}{|Z_{G_k}|^2})^2 + (Q_{G_k} + \frac{Tr\{M_k W\}X_{G_k}}{|Z_{G_k}|^2})^2 \ge Tr\{M_k W\}(\frac{V_{C_k}^{min}}{|Z_{G_k}|})^2 \tag{12}$$

Schur's complement method is used to reformulate (10) and (11) as negative semidefinite constraints. For (10) the negative semidefinite constraint is written as,

$$\begin{bmatrix} -Tr\{M_k W\}(I_{C_k}^{max})^2 & A_i & B_i \\ A_i & -1 & 0 \\ B_i & 0 & -1 \end{bmatrix} \le 0 \tag{13}$$

where $A_i = P_{G_k}$ and $B_i = Q_{G_k}$. Similarly for (11) the negative semidefinite Schur's complement is,

$$\begin{bmatrix} -Tr\{M_k W\}(\frac{V_{C_k}^{max}}{|Z_{G_k}|})^2 & A_v & B_v \\ A_v & -1 & 0 \\ B_v & 0 & -1 \end{bmatrix} \le 0 \tag{14}$$

where $A_v = P_{G_k} + \frac{Tr\{M_k W\}R_{G_k}}{|Z_{G_k}|^2}$ and $B_v = Q_{G_k} + \frac{Tr\{M_k W\}X_{G_k}}{|Z_{G_k}|^2}$.

Prima facie the minima in (12) can be converted to a maximum by inversion,

$$-(P_{G_k} + \frac{Tr\{M_k W\}R_{G_k}}{|Z_{G_k}|^2})^2 - (Q_{G_k} + \frac{Tr\{M_k W\}X_{G_k}}{|Z_{G_k}|^2})^2 \le -Tr\{M_k W\}(\frac{V_{C_k}^{min}}{|Z_{G_k}|})^2$$

and Schur's complement for the above equation is,

$$\begin{bmatrix} Tr\{M_k W\}(\frac{V_{C_k}^{min}}{|Z_{G_k}|})^2 & -A_v & -B_v \\ -A_v & 1 & 0 \\ -B_v & 0 & 1 \end{bmatrix} \le 0$$

It should be noticed that the complement does not satisfy the conditions for a negative semidefinite matrix as the first principal minor is positive. Hence, the constraint in (12) needs to be approximated on a case-to-case basis. Since the reactive power constraint depends on two variables, a piece-wise planar approximation is proposed in this work.

The set of active powers generation is divided into subsets multiple subsets. It is assumed that the function $Q_{G_k}(P_{G_k}, V_{G_k}^2)$ is parallel in the intervals $\{[p_0, p_1), [p_1, p_2), \dots [p_i, p_i + 1)\dots\}$ with respect to the variable $V_{G_k}^2$. This is a strong assumption for the planar surface; nonetheless, the piece-wise planar approximation is empirically validated to result in an error of less than ±5% with the active power range divided into three subsets. The above statement is valid for all reasonably designed converters satisfying the grid code requirements [9].

The lower voltage constraint is approximated by a piece-wise planar approximation within the defined sets of active power generation as follows,

$$Q_{G_k} \ge \begin{cases} a_1 P_{G_k} + b_1 V_{G_k}^2 + c_1, & \text{if } p_0 < P_{G_k} < p_i; \forall V_{G_k}^2 \\ \dots \\ a_i P_{G_k} + b_i V_{G_k}^2 + c_i, & \text{if } p_i < P_{G_k} < p_{i+1}; \forall V_{G_k}^2 \\ \dots \\ \dots \end{cases} \tag{15}$$

Re-writing the piece-wise planar approximation in terms of the optimization variable W,

$$Q_{G_k} \geq \begin{cases} a_1 P_{G_k} + b_1 Tr\{M_k W\} + c_1, & \text{if } p_0 < P_{G_k} < p_i; \forall W \\ \dots \\ a_i P_{G_k} + b_i Tr\{M_k W\} + c_i, & \text{if } p_i < P_{G_k} < p_{i+1}; \forall W \\ \dots \\ \dots \end{cases} \tag{16}$$

Note that another underlying assumption behind the planar approximation is that the converters connecting RES are operated in an active power priority mode, which implies that the active power is not curtailed.

3. Application study 1: Reactive power constraints for WPP

This section quantifies the feasible reactive power set and tests the accuracy of the planar approximation for two different WPPs.

3.1. Quantification of feasible reactive power set

An exemplary WPP is considered to quantify the feasible reactive power set. The parameters of the individual wind turbine generators are taken from [36], which specifies that the GSC is 25% oversized. The maximum rated current for the GSC is 1.25 p.u., while the maximum and minimum voltages are 1.1 p.u. and 0.8 p.u. respectively. A single wind turbine has 0.84% resistance and 5% impedance, and the reactance of the filter and the power line is 8.5%. The WPP is comprised of five wind turbines connected parallelly. The equivalent impedance of the WPP, considering the collector system is derived analytically based on the method in [59].

The reactive power from the WPP connected with GSC is a function of the active power generated and voltage at the point of connection according to (8) and (9). Let the maximum and minimum values for the reactive power from (8) and (9) be defined as follows,

$$Q_{I_{C_k},max} = +\sqrt{V_k I_{C_k}^{max} - P_{G_k}^2}$$

$$Q_{I_{C_k},min} = -\sqrt{V_k I_{C_k}^{max} - P_{G_k}^2}$$

$$Q_{V_{C_k},max} = \sqrt{\left(\frac{V_k V_{C_k}^{max}}{|Z_{G_k}|}\right)^2 - \left(P_{G_k} + \frac{V_k^2 R_{G_k}}{|Z_{G_k}|^2}\right)^2} - \frac{V_k^2 X_{G_k}}{|Z_{G_k}|^2}$$

$$Q_{V_{C_k},min} = \sqrt{\left(\frac{V_k V_{C_k}^{min}}{|Z_{G_k}|}\right)^2 - \left(P_{G_k} + \frac{V_k^2 R_{G_k}}{|Z_{G_k}|^2}\right)^2} - \frac{V_k^2 X_{G_k}}{|Z_{G_k}|^2}$$

The limits on reactive power are written as follows,

$$max(Q_{I_{C_k},min}, Q_{V_{C_k},min}) \leq Q_{G_k} \leq min(Q_{I_{C_k},max}, Q_{I_{C_k},max})$$

The total feasible reactive power set for the range of permissible voltage at the point of connection and active power generation is measured by an index QS representing the area of the feasible set.

$$QS = \int_{0.9}^{1.1} \int_{0}^{1} |min(Q_{I_{C_k},max}, Q_{I_{C_k},max}) - max(Q_{I_{C_k},min}, Q_{V_{C_k},min})| d P_{G_k} d V_k$$

The index QS representing the area of the feasible reactive power set is calculated and compared for three different cases,

- QS1: Minimum required grid codes requirements as limits on reactive power
- QS2: Only maximum current limit on reactive power–(8)
- QS3: Maximum converter current and maximum and minimum voltage limits on reactive power–(8) and (9)

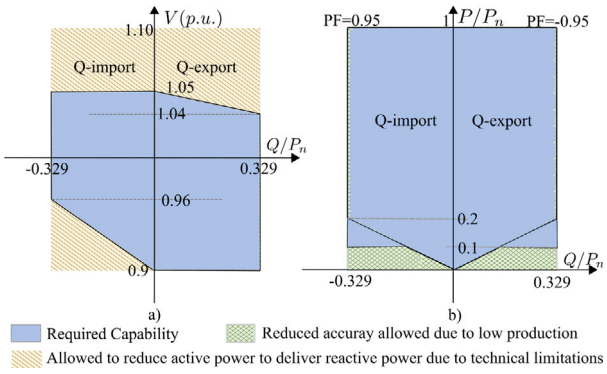

Fig. 3. Requirements for the supply of reactive power at (a) maximum active power generation; (b) different active power levels [60].

Grid Code Requirements (GCR)

The EU Commission Regulation for connection of generators categorizes converter-connected generators into four categories based on their installed capacity [9]. The exemplary WPP falls under the Type D RES. The grid codes specify the required reactive power capability at different voltages and active power production at the point of connection for a Type D RES as illustrated in Fig. 3.

The feasible reactive power set QS3 is considered the benchmark set. The EU Commission Regulation for connection of generators (with Danish implementation) requirements restrict the total feasible set QS1 to approximately 39.2% of QS3 indicating the underutilized potential of the reactive power capabilities of a converter-connected WPP.

Fig. 4 shows the feasible reactive power space for the WPP at two different voltages. Notice that the maximum and minimum voltage constraint ($Q_{V_{C_k},max}$ and $Q_{V_{C_k},min}$) further reduce the reactive power set within the current constraint ($Q_{I_{C},max}, Q_{I_{C},min}$). Thus, the set QS2 over-estimates the reactive power capability by 130% (QS3/QS2).

3.2. Accuracy of the planar approximations

The accuracy of the planar approximation is tested on two different WPP systems. The first WPP system, WPP-A, consists of five wind turbines with a rated capacity of 3 MW each connected in parallel, and the second WPP, WPP-B, with 15 wind turbines, with a total capacity of 45 MW. The equivalent impedance and filter design parameters for WPP-A and WPP-B are derived from [36,59].

The upper and lower limit for reactive power defined by (9) is depicted in Fig. 5 for both WPP-A and WPP-B. The GSC in WPP-A is oversized enabling it to provide more reactive power support to the grid, whereas the GSC in WPP-B is not oversized. The difference in the available feasible reactive power for WPP-A and WPP-B can be seen on comparing the two subplots in Fig. 5. Albeit, the voltage constrained lower bound for reactive power from WPPs is a quadratic function of the active power generation and voltage at the point of coupling, the radius of this circle is large. A judiciously calculated piece-wise planar function thus serves a reasonable convex approximation for the non-convex lower bound voltage constraint.

A three-piece-wise planar approximation for the lower voltage limit constraint on reactive power is compared with a single planar approximation to demonstrate the advantage of the piece-wise planar approach. Fig. 6 shows the approximation overlaid with the original constraint together with the percentage error for both approximations. The percentage error plot depicts the mismatch between the original and the planar approximation at each point.

The maximum mismatch between the original and the approximation in the planar approximation is 0.09 MVAR which accounts for a difference of 8.5%. The single planar approximation is not able to capture the non-linearity of the quadratic constraint equation. Whereas,

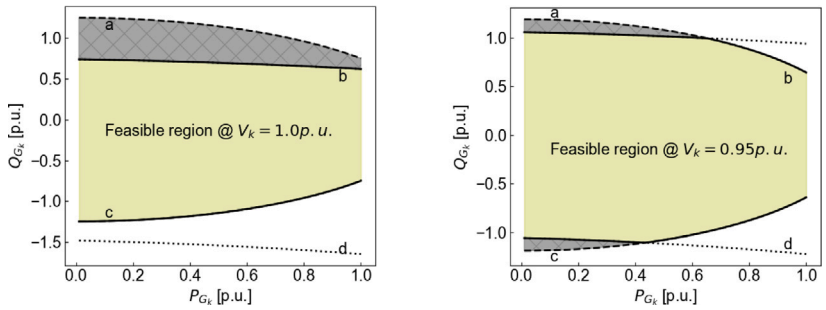

Fig. 4. Feasible Reactive Power Set at Voltage (a) V_k = 1.0 p.u. (b) V_k= 0.95 p.u. | Indicators in the figure a: $Q_{I_c,max}$; b: $Q_{V_{c_k},max}$; c: $Q_{I_c,min}$; d: $Q_{V_{c_k},min}$.

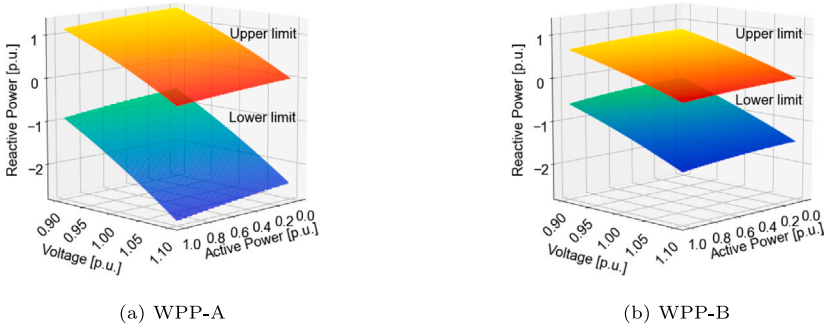

Fig. 5. Converter constraints on reactive power at different values of connection voltage $|V_{G_k}|$ and active power output P_{G_k}.

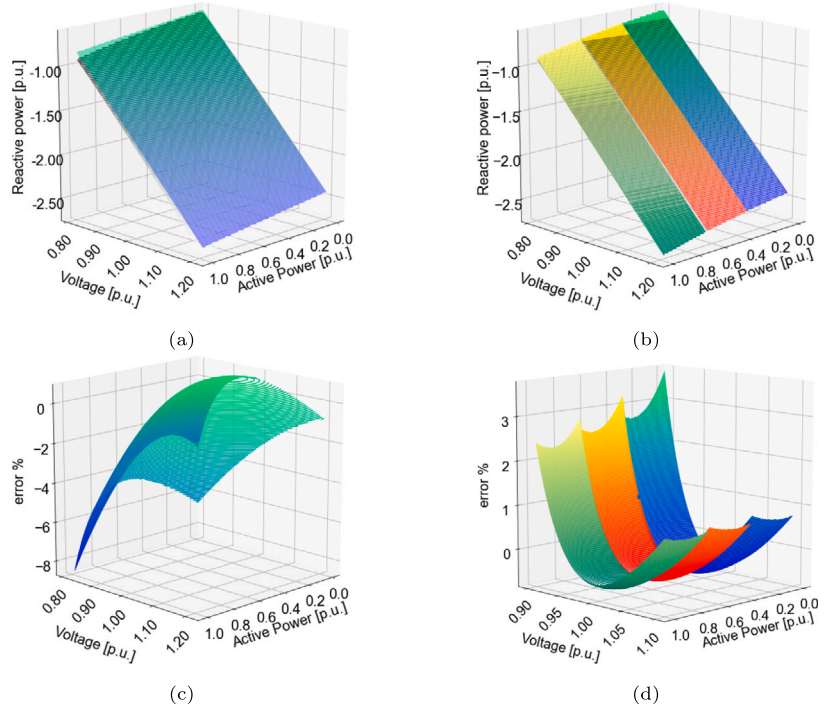

Fig. 6. Planar approximation and percentage errors for WPP-A (a) single plane approximation (b) three piece-wise planar approximation (c) the Percentage error in single planar approximation (d) the Percentage error in three piece-wise planar approximation.

the three-planar approximation computes three different slopes closely capturing the non-linearity of the constraint. The maximum mismatch in the three piece-wise planar approximations is 0.024 MVAR or 3.7%. Similarly for WPP-B, the maximum mismatch with a single plane approximation is 0.05 MVAR or 8.16%. The maximum mismatch between the planar approximation and the quadratic constraint reduces to 0.021 MVAR with three piece-wise planar approximations. The data is tabulated in Table 1.

Table 1
Maximum error in piece-wise planar approximation.

	Single Plane		Three Planes	
	[%]	[MVAR]	[%]	[MVAR]
WPP-A	8.5	0.09	3.7	0.024
WPP-B	8.16	0.05	3.6	0.021

The three-piecewise planar approach can thus be used to emulate the lower voltage reactive power constraints on WPPs in a distribution network using SDP. A medium voltage balanced distribution network with a large share of WPPs is chosen for the application as described in the following section.

4. Application study 2: WPPs as reactive power source in distribution network

This section highlights key results from deploying the reactive power capabilities of WPP in a distribution network with the proposed method to incorporate the converter model. Firstly, the distribution network data is briefly introduced, and an assessment of the duality gap is presented to establish the validity of the solutions and global minima from the presented method. Secondly, the reactive power provided by the WPPs in all three cases is analysed along with the reactive power flow between the transmission and distribution network. Finally, the effect of local reactive power supply on the distribution network operation is studied by comparing active power loss and voltage profile in the network amongst the cases. The analysis is conducted with respect to the earlier defined reactive power feasibility sets, QS1, QS2, and QS3, which are benchmarked against a base case where no reactive power contribution from RES is considered.

The proposed framework is programmed in Python with the CVXPY library used to model the semidefinite constraints. The optimization is solved in a cluster computer at the Technical University of Denmark [61] using the MOSEK solver. The distribution grid data along with the load and generation time series is completely open-source [62].

4.1. Distribution grid data

A network model from a real Danish medium voltage distribution network is used to assess the performance of the proposed method to incorporate converter constraints in the convex SDP model along with the three feasible reactive power sets. Load and generation profiles for over 10 months are available with the network data. Thus, the reactive power capability constraints are demonstrated in a variety of different load and generation scenarios.

The layout of the 60 kV distribution network, depicted in Fig. 7, is briefly described in this section. Further details can be found in [6, 62]. The network is connected to the high voltage (HV) transmission network through one step-up 60 /150 kV transformer, and to the low voltage (LV) 10 kV buses through several step-down 60 /10 kV transformers at all the depicted buses. The step-up 60 /150 kV transformer forms the interface between the transmission system operator (TSO) and the DSO. The three wind power plants (WPPs) connected at 60 kV serves as the converter-connected weather-dependent generation for this case. The WPPs have installed capacities of 12 MW, 15 MW, and 15 MW, respectively.

The salient features of this network are shown in Table 2. It should be mentioned that approximately one year of SCADA measurements with a one-hour resolution is available for the present investigation.

The network data presented, along with load and generation profiles is part of an open-source multi-voltage balanced distribution network called DTU-7k Bus Active Distribution Network [62].

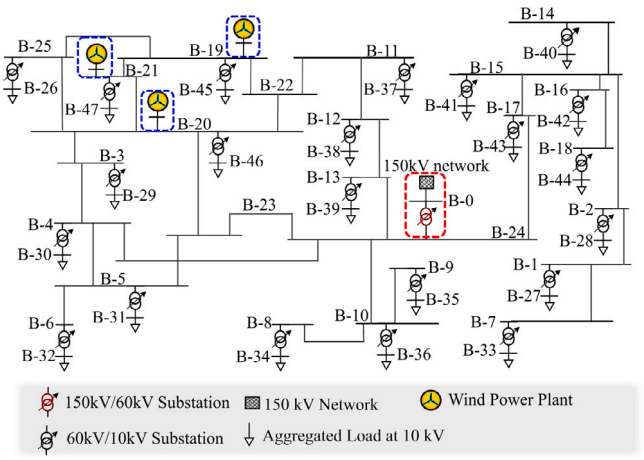

Fig. 7. Layout for the 60 kV distribution network.

Table 2
The 60 kV distribution network.

Network Element	#	Voltage Level
Buses	25	60 kV
TSO/DSO substation	1	150 kV/60 kV
Substations with uncontrollable generation	13	60 kV/10 kV
Substations with controllable generation	3	60 kV/10 kV
Transformers	1	150 kV/60 kV
	22	60 kV/10 kV
Type IV controllable WPPs	3	60 kV
Loads (Aggregated)	22	10 kV

Table 3
Case description.

Name	Feasible Reactive Power Set
Base Case	[0] Zero reactive power support
WPP(QS1)	Danish Grid Codes
WPP(QS2)	Only current constraint on GSC - (8)
WPP(QS3)	Current and voltage constraints on GSC - (8), (9)

4.2. Case descriptions

Four cases are defined in this study differing in the feasible reactive power available from the WPPs tabulated in Table 3.

4.3. Duality gap analysis

The duality gap between the classical optimization and dual of the convex relaxation via SDP is zero if and only if the optimal matrix is positive semidefinite and its nullspaces have dimensions less than or equal to two [48,50]. This condition is satisfied at all time stamps for both the cases WPP(GCR) and WPP(CC).

Due to numerical uncertainties, the rank condition for the duality gap may not be satisfied. Hence authors in [50] proposes two different criteria to evaluate the duality. The first proposed criterion is the minimum eigenvalue ratio, evaluated between the 2nd and 3rd minimum eigenvalues. The minimum eigenvalue ratio for WPP(GCR) and WPP(CC) is obtained in the range $10^{8} - 10^{14}$, which satisfies the duality gap criteria specified in [50].

The second criterion proposed in [50] is the mismatch between the active and reactive power values at the load buses. The mismatch is for WPP(GCR) and WPP(CC) is less than 10^{-2}. This also indicates satisfactory convergence of the SDP relaxation approach with the proposed converter models. According to [48,50], the convergence of the optimization can be enforced by adding a minimum resistance of 10^{-4} to the lines. However, this is not necessary for the presented dataset as the lines in the distribution grid already have considerable resistance.

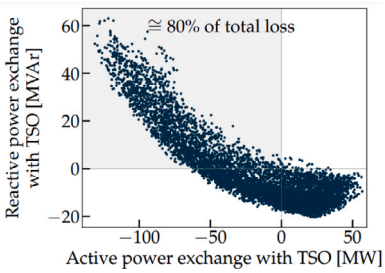

Fig. 8. Active and Reactive power flow at the transmission–distribution interface for Base Case.

4.4. Reactive power support from WPPs in a distribution network

The aggregated loads in the distribution network have negative values for more than 50% of the simulated time, indicating a high penetration of distributed generation in the low-voltage networks. Notice from Fig. 8 the distribution network has a high reverse power flow. Power flowing from the transmission to the distribution network is considered positive and the reverse power flow is negative. During the reverse power flow, the distribution network needs to import high amounts of reactive power from the transmission network.

Part of the reactive power imported from the transmission network is to be supplied by the WPPs in all three cases. In the case of WPP(QS1), the reactive power from the WPPs is restricted to 0.329% of their installed capacities. It is observed that in the case of WPP(QS1), the WPPs supply reactive power at the upper limit of the feasible set QS1 when the active power generation is high (See Fig. 9(a)).

The reactive power set point for the individual WPPs depends on the network topology, the amount of active and reactive power demand, as well as the location of the WPP in the network. The focus of the algorithm is not on the equitable distribution of reactive power amongst available WPPs to impact their internal losses or revenue from the reactive power supply if any. Thus in the case of WPP(QS2), when the WPPs are limited only by the maximum current limit of the GSC, WPP-1 and WPP-2 are observed to supply the bulk of the reactive power required for the optimization as plotted in Fig. 9(b). In comparison, when the complete converter model is used in WPP(QS3), the voltage limits of GSC restrict reactive power from WPP-1 and WPP-2. Notice from Fig. 9(c) that WPP-3 supplies part of the reactive power in conjunction with WPP-1 and WPP-2. Also notice that the maximum reactive power supplied by the three WPPs combined is around 20 MVar in WPP(QS2) and 15 MVar in WPP(QS1) as opposed to 17 MVar in WPP(QS3). The different peaks for combined reactive power supply from the WPPs demonstrate that using only the maximum current constraint for GSC overestimated the available reactive power capabilities from RES and the grid code requirements underutilized the reactive power capability validating the proposed hypothesis. Moreover, it is found that the GSC constraints are violated for 22% of the timestamps in WPP(QS2), indicating that using only the apparent power constraints would provide infeasible reactive power set points for the WPPs for the number of timestamps equivalent to over 2 months.

4.5. Reactive power flow at the transmission–distribution interface

The local supply and consumption of reactive power in the distribution grid also affect the reactive power flow across the 60 kV/150 kV transformer, which is the transmission–distribution interface.

From Fig. 10 it is observed that the reactive power demand of the distribution network from the transmission grid is lower in all three simulated cases. A similar effect is observed in the reverse reactive power flow from the distribution to the transmission grid but with diminished intensity.

Table 4
Reactive power flow at the reference node.

	T → D [%]	D → T [%]
Base Case	100	100
WPP(QS1)	44.5	79.5
WPP(QS2)	19.5	82.8
WPP(QS3)	39	80.2

Table 5
Total Energy loss and loss reduction in all cases.

	Energy loss [MWh]	Δ Loss [MWh]	% Reduction –
Base Case	6742	0	0
WPP(QS1)	6487	255	3.8
WPP(QS2)	6423	319	4.7
WPP(QS3)	6466	276	4.1

Table 4 quantifies the reactive power flow across the reference node as a percentage of the reactive power flow in the Base Case. The table confirms the observation from Fig. 10 of a drastic reduction in the reactive power flow from the transmission to the distribution network in WPP(QS1), WPP(QS2), and WPP(QS3) cases which is calculated to 44.5%, 19.5%, and 39% of the Base Case respectively. The reverse reactive power flow from distribution to the transmission grid is also reduced to 79.6%, 82.8%, and 80.2% of the Base Case for the three cases. Notice that the maximum required reactive power from the transmission network in the Base Case is 60 MVar, which is reduced to 45 MVar in WPP(QS1) and 40 MVar in WPP(QS3). Since the case WPP(QS2) overestimates the local reactive power availability, it produces a false maximum reactive power of 30 MVar which is lower than the real value, indicating the error induced on system operation by partial modelling of the reactive power potential from RES.

Thus, the distribution network presented here is able to locally satisfy approximately 50% of its reactive power requirement from the installed converter-connected WPPs for the period of a year. Assuming that instead of using the reactive power from converter-connected WPPs, a 20 MVar capacitor bank or other reactive power sources is installed to provide the same amount of reactive power. The cost of the reactive power source would be greater than approximately 200 k€. The cost of a reactive power source is an approximate estimate from various vendors and web shops and can vary from region to region. Thus, local reactive power from converter-connected RES saves expensive grid reinforcements.

It can be argued that the internal losses for the RES increase as they are deployed to provide reactive as well as active power. The total loss in a WPP, according to [41], is approximately 5% for 0.33 p.u. of reactive power from the WPP and about 4.5% of the total active power generated per year for the same WPP. While authors in [39], calculated the total increase in losses for a PV plant at a maximum of 5.6%. A comparison for the compensation cost to the RES operators cannot be directly made as reactive power markets and compensation is not well established to date and continues to be a topic under research.

4.6. Improved energy loss reduction

Approximately 80% of the total active power loss in the considered distribution network occurs over the time stamps with high reverse power flow. By supplying part of the reactive power demand locally, the current required to transfer the same amount of active power is reduced, and in consequence the line losses, as they are dependent on the square of the current.

As tabulated in Table 5, WPP(QS1) results in an energy loss reduction of 255 MW equating to 3.8% less than the base case. While WPP(QS3) results in an energy loss reduction of 4.1% which is comparable to WPP(QS2) at a reduction of 4.7%, due to the redistribution

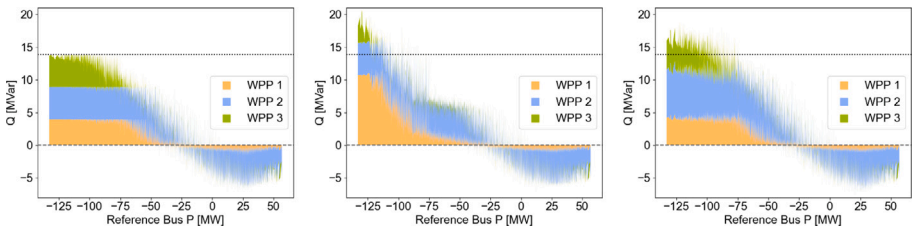

Fig. 9. Stacked plot of reactive power from three WPPs with respect to the active power at reference node for (a) WPP(QS1); (b) WPP(QS2); (c) WPP(QS3).

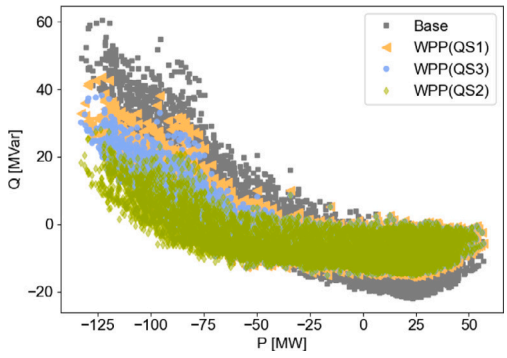

Fig. 10. Active and Reactive Power Flow at reference node.

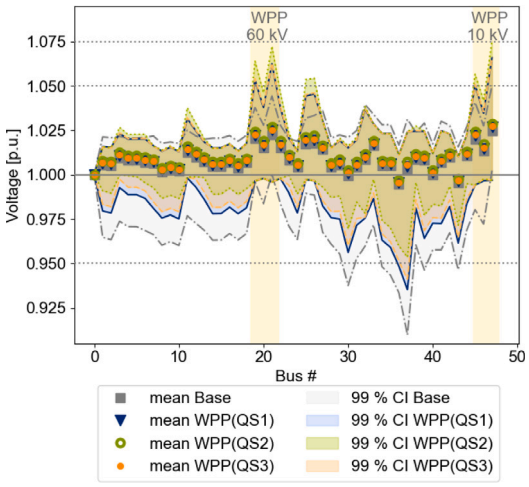

Fig. 11. Distribution of voltage profile at each node in the distribution grid. *WPP 60 kV* highlights the substation where the WPPs are connected, whereas *WPP 10 kV* is the 10 kV side of the same substation [CI: Confidence Interval].

of reactive power capabilities amongst the three available WPPs in WPP(QS3).

It is noted that the results of this new proposed dual optimization problem are much better compared to the results of the genetic algorithm-based optimization, implemented on the same distribution grid dataset and described in a previous work [63]. In [63], it was shown that the energy saving achieved by using the heuristic optimization is 103 ± 2.92 MWh, approximately 1.5% less than the base case losses. This direct comparison highlights the ability of the SDP approach to find a global optimum in contrast to a heuristic optimization.

The generation and load profiles used for the simulation are from the year 2015 when the electricity price averaged at approximately 0.33 €/kWh [64]. Even if all the RES in the given network model provide the minimum required reactive power (WPP(QS1)) according to the grid codes, total active power savings are calculated to be 84 k€. In contrast, if the RES operate at their full reactive power capability (WPP(QS2)) to optimize the distribution network, the total active power savings increase to 91 k€, which is 8% more than WPP(QS1) case. Thus, converter-connected RES as local reactive power sources result in direct monetary benefits for the distribution network.

4.7. Improved voltage profile in the distribution network

The voltage at any bus in the distribution grid depends on the reactive power support and the node's load. Since the case study simulates a time series of over a year, portraying the voltage profile at a single time stamp does not justify the total effect of locally supplying reactive power in the distribution grid. Hence, Fig. 11 plots the voltage distribution at each bus for all the time stamps picturing the mean, median, and the 99^{th} percentile region.

As depicted in Fig. 11, the voltage profile in the distribution network improves with the local reactive power support from WPPs. The maximum increase in voltages is observed at buses 19, 20, and 21 where WPPs are connected. It is to be noted that these buses also host a 60 kV/10 kV distribution transformer. The 10 kV side of the distribution transformer is also highlighted in Fig. 11 at buses 45, 46, and 47 which also show a high increase in the mean value of the voltage profile. The increase in voltage profiles is less in WPP(QS1) and WPP(QS3) in comparison to WPP(QS2); however, the voltage profile distribution reveals the fact that local reactive power supply can have a positive impact on the voltage profiles in all load and generation scenarios.

5. Conclusion

The principal aim of this research is the extensive utilization of reactive power capability offered by converter-connected renewable energy sources (RES). The grid code requirements under-utilize the available reactive power from RES. While modelling the reactive power capability from RES using only the apparent power constraint overestimates the reactive power from RES. This research models the reactive power from the converter-connected RES using three sets of constraints based on the maximum rated current and maximum and minimum rated grid-side converter voltage. The three approaches for modelling the reactive power from RES, i.e. with grid code requirements, using only apparent power constraint, and the complete converter model, are compared using a reactive power area measurement index. It is found that the grid code requirements use only 39% of the available reactive power potential while using only the apparent power constraint overestimates the available reactive power up to 130%. It is hypothesized inaccurate and insufficient quantification of the available reactive power potential can be detrimental for system operations and give erroneous results in studies that focus on utilizing RES reactive power capability to avoid grid reinforcements or enable an active role for distribution networks.

To further emphasize the importance of accurately modelling the reactive power from RES, a power flow optimization study is conducted with reactive power from RES as a variable for the optimization. A

novel method to incorporate the non-linear and non-convex converter equations in a convex semidefinite programming (SDP) based power flow optimization framework is proposed. The non-linear but convex converter constraints are reformulated using Schur's complement method to be included in the SDP model. A piece-wise planar approximation is proposed for the non-convex converter constraint. The accuracy of the proposed approximation is demonstrated using two different wind power plant (WPP) equivalent circuits. The non-convex converter equations are approximated within an error of less than 4% with a three-piece-wise planar approximation.

The SDP model with the reformulated and approximated converter constraints remains essentially convex and thus guarantees a globally optimal solution. The choice of a convex optimization ensures maximum reactive power contribution from the converter-connected RES for the optimization objective. The presented investigation has shown that the SDP model with the converter constraint equations converges to a global optimum with a zero duality gap.

The algorithm is implemented on a real distribution network model with WPPs as converter-connected RES. The simulation is performed with realistic load and generation time series for over 10 months, thus facilitating a variety of load versus generation scenarios. The simulation results quantify the under-utilization of the available reactive power capabilities using the minimum grid code requirements. It is observed that the peak reactive power support from WPPS in the distribution network is 15 MVar with grid code requirements, and 20 MVar with partial modelling using only the apparent power constraints. However, the proposed model for converter-connected RES outputs the peak reactive power at 17 MVar, thus establishing the under-utilization and overestimation of available reactive power capabilities. A similar discrepancy is observed when quantifying the reactive power dependence of the distribution network on the transmission network.

Furthermore, the benefits of using local reactive power in a distribution network are reiterated and compared in this work with all three different feasible reactive power sets. The dependence of the distribution network on the transmission network for reactive power declined by 50% while improving the voltage profile in all load versus generation scenarios. A 4.1% reduction in active power losses is observed over a period of 10 months.

CRediT authorship contribution statement

Aeishwarya Baviskar: Conceptualization, Methodology, Software, Validation, Formal analysis, Investigation, Writing – original draft, Visualization. **Anca D. Hansen:** Conceptualization, Methodology, Resources, Writing – review & editing, Supervision, Funding acquisition, Project administration. **Kaushik Das:** Conceptualization, Methodology, Resources, Writing – review & editing, Supervision. **Firdous Ul Nazir:** Conceptualization, Methodology, Writing – review & editing, Supervision.

Declaration of competing interest

The authors declare that they have no known competing financial interests or personal relationships that could have appeared to influence the work reported in this paper.

Data availability

Data will be made available on request

Acknowledgements

This project has received funding from the European Union's Horizon 2020 research and innovation programme under the Marie Sklodowska-Curie grant agreement No 861398 and Energy Technology Development and Demonstration Programme (EUDP) 2019-II IEA Task 41 Journal Number 64019-0518.

References

[1] Henderson MI, Novosel D, Crow ML. Electric power grid modernization trends, challenges, and opportunities. IEEE Technol Trend Paper 2017;(November):17.
[2] Deloitte, EDSO, Eurelectric. Connecting the dots: Distribution grid investment to power the energy transition. 2021, p. 76.
[3] Gautam K, Purkayastha D. The future of distributed renewable energy in India. Tech. Rep., (May). Climate Policy Initiative; 2021, URL https://www.climatepolicyinitiative.org.
[4] Allen A, Allen A. Voltage impacts of utility-scale distributed wind voltage impacts of utility- scale distributed wind. (September). 2014.
[5] Danish Energy Agency. Development and role of flexibility in the danish power system - solutions for integrating 50% wind and solar, and potential, future solutions for the remaining 50%. Tech. Rep., (June). Danish Energy Agency; 2021, (Under development).
[6] Baviskar A, Hansen AD, Das K, Koivisto M. Challenges of future distribution systems with a large share of variable renewable energy sources – review. In: 19th wind integration workshop 2020. (November). 2020.
[7] Alboaouh KA, Mohagheghi S. Impact of rooftop photovoltaics on the distribution system. J Renew Energy 2020;2020:1–23. http://dx.doi.org/10.1155/2020/4831434.
[8] Xue Y, Sharma I, Kuruganti T, Nutaro J, Dong J, Olama M, et al. Voltage impact analyses of solar photovoltaics on distribution load tap changer operations. In: 2017 north American power symposium, NAPS 2017. 2017, http://dx.doi.org/10.1109/NAPS.2017.8107252.
[9] ENTSO-E. Commission Regulation (EU) 2016/631 of 14 April 2016 establishing a network code on requirements for grid connection of generators. Off J Eur Union 2016;(14 April 2016):1–68.
[10] Energinetdk. Technical regulation 3.2.2 for PV power plants above 11 kW. 2016, p. 1–108.
[11] Federal energy regulatory commission. Order 2222: Participation of distributed energy resources aggregations in markets operated by RTO and ISO. 2021.
[12] Cabadag RI, Schmidt U, Schegner P. The voltage control for reactive power management by decentralized wind farms. In: 2015 IEEE eindhoven PowerTech, PowerTech 2015. IEEE; 2015, p. 1–6. http://dx.doi.org/10.1109/PTC.2015.7232588.
[13] Yang F, Li Z. Improve distribution system energy efficiency with coordinated reactive power control. IEEE Trans Power Syst 2016;31(4):2518–25. http://dx.doi.org/10.1109/TPWRS.2015.2477378.
[14] Stock DS, Venzke A, Lower L, Rohrig K, Hofmann L. Optimal reactive power management for transmission connected distribution grid with wind farms. In: IEEE PES innovative smart grid technologies conference Europe. 2016, p. 1076–82. http://dx.doi.org/10.1109/ISGT-Asia.2016.7796535.
[15] Soroudi A, Rabiee A, Keane A. Distribution networks' energy losses versus hosting capacity of wind power in the presence of demand flexibility. Renew Energy 2017;102:316–25. http://dx.doi.org/10.1016/j.renene.2016.10.051.
[16] Tahir M, El Shatshat RA, Salama MM. Reactive power dispatch of inverter-based renewable distributed generation for optimal feeder operation. In: 2018 IEEE electrical power and energy conference, EPEC 2018. IEEE; 2018, p. 1–6. http://dx.doi.org/10.1109/EPEC.2018.8598376.
[17] Dong J, Xue Y, Olama M, Kuruganti T, Nutaro J, Winstead C. Distribution voltage control: Current status and future trends. In: 2018 9th IEEE international symposium on power electronics for distributed generation systems, PEDG 2018. IEEE; 2018, http://dx.doi.org/10.1109/PEDG.2018.8447628.
[18] Nazir FU, Pal BC, Jabr RA. Distributed solution of stochastic volt/VAr control in radial networks. IEEE Trans Smart Grid 2020;11(6):5314–24. http://dx.doi.org/10.1109/TSG.2020.3002100.
[19] Tang Z, Hill DJ, Liu T. Distributed coordinated reactive power control for voltage regulation in distribution networks. IEEE Trans Smart Grid 2021;12(1):312–23. http://dx.doi.org/10.1109/TSG.2020.3018633.
[20] Potter A, Haider R, Annaswamy AM. Reactive power markets for the future grid. 2021, URL http://arxiv.org/abs/2110.02337.
[21] Das K, Martinez EN, Altin M, Hansen AD, Sorensen PE, Thybo GW, et al. Facing the challenges of distribution systems operation with high wind power penetration. In: 2017 IEEE manchester PowerTech, Powertech 2017. 2017, http://dx.doi.org/10.1109/PTC.2017.7981136.
[22] Kraiczy M, Wang H, Schmidt S, Wirtz F, Braun M. Reactive power management at the transmission-distribution interface with the support of distributed generators - A grid planning approach. IET Gener, Transm Distribution 2018;12(22):5949–55. http://dx.doi.org/10.1049/iet-gtd.2018.5673.
[23] Sirviö K, Mekkanen M, Kauhaniemi K, Laaksonen H, Salo A, Castro F, et al. Controller development for reactive power flow management between DSO and TSO networks. In: Proceedings of 2019 IEEE PES innovative smart grid technologies Europe, ISGT-Europe 2019. Institute of Electrical and Electronics Engineers Inc.; 2019, http://dx.doi.org/10.1109/ISGTEurope.2019.8905578.

[24] Dong L, Tian AZ, Pu TJ, Fan Z, Yu T. Reactive power optimization for distribution network with distributed generators based on semi-definite programming. Adv Mater Res 2014;1070–1072:809–14. http://dx.doi.org/10.4028/www.scientific.net/amr.1070-1072.809.

[25] Yuan R, Li T, Deng X, Ye J. Optimal day-ahead scheduling of a smart distribution grid considering reactive power capability of distributed generation. Energies 2016;9(5). http://dx.doi.org/10.3390/en9050311.

[26] Majumder S, Khaparde SA. Revenue and ancillary benefit maximisation of multiple non-collocated wind power producers considering uncertainties. IET Gener Transm Distrib 2016;10(3):789–97. http://dx.doi.org/10.1049/iet-gtd.2015.0480, URL https://onlinelibrary.wiley.com/doi/10.1049/iet-gtd.2015.0480.

[27] Rezaei F, Esmaeili S. Decentralized reactive power control of distributed PV and wind power generation units using an optimized fuzzy-based method. Int J Electr Power Energy Syst 2017;87:27–42. http://dx.doi.org/10.1016/j.ijepes.2016.10.015, URL https://linkinghub.elsevier.com/retrieve/pii/S0142061515301137.

[28] Luo L, Gu W, Zhang X-P, Cao G, Wang W, Zhu G, et al. Optimal siting and sizing of distributed generation in distribution systems with PV solar farm utilized as STATCOM (PV-STATCOM). Appl Energy 2018;210:1092–100. http://dx.doi.org/10.1016/j.apenergy.2017.08.165, URL https://linkinghub.elsevier.com/retrieve/pii/S0306261917311844.

[29] Li J, Xu Z, Zhao J, Zhang C. Distributed online voltage control in active distribution networks considering PV curtailment. IEEE Trans Ind Inf 2019;15(10):5519–30. http://dx.doi.org/10.1109/TII.2019.2903888.

[30] Teshome DF, Xu W, Bagheri P, Nassif A, Zhou Y. A reactive power control scheme for DER-caused voltage rise mitigation in secondary systems. IEEE Trans Sustain Energy 2019;10(4):1684–95. http://dx.doi.org/10.1109/TSTE.2018.2869229, https://ieeexplore.ieee.org/document/8457299/.

[31] Karagiannopoulos S, Mylonas C, Aristidou P, Hug G. Active distribution grids providing voltage support: The swiss case. IEEE Trans Smart Grid 2020;12(1):268–78. http://dx.doi.org/10.1109/TSG.2020.3010884, URL https://ieeexplore.ieee.org/document/9145713/.

[32] Gandhi O. Reactive power support using photovoltaic systems. 2021, URL http://link.springer.com/10.1007/978-3-030-61251-1.

[33] Hashemipour N, Aghaei J, Niknam T, Shafie-Khah M, Wang F, Catalão JP. Voltage profile optimization with coordinated control of PV inverters. In: 21st IEEE international conference on environment and electrical engineering and 2021 5th IEEE industrial and commercial power system Europe, EEEIC / I and CPS Europe 2021 - proceedings. Institute of Electrical and Electronics Engineers Inc.; 2021, http://dx.doi.org/10.1109/EEEIC/ICPSEurope51590.2021.9584552.

[34] Ul Nazir F, Pal BC, Jabr RA. Affinely adjustable robust volt/VAr control without centralized computations. IEEE Trans Power Syst 2022. http://dx.doi.org/10.1109/TPWRS.2022.3158816.

[35] Liu MZ, Ochoa LF, Low SH. On the implementation of OPF-based setpoints for active distribution networks. IEEE Trans Smart Grid 2021;12(4):2929–40. http://dx.doi.org/10.1109/TSG.2021.3054387.

[36] Sarkar M, Altin M, Sørensen PE, Hansen AD. Reactive power capability model of wind power plant using aggregated wind power collection system. Energies 2019;12(9). http://dx.doi.org/10.3390/en12091607.

[37] Albarracin R, Alonso M. Photovoltaic reactive power limits. In: 12th international conference on environment and electrical engineering, EEEIC 2013. 2013, p. 13–8. http://dx.doi.org/10.1109/EEEIC.2013.6549630.

[38] Yuan B, Xu J, Zhao C. Systems steady-state analysis of voltage source converter (VSC) connected to weak AC system and optimal control strategies steady-state analysis of voltage source converter (VSC) connected to weak AC system and optimal control strategies. Electr Power Compon Syst 2018;46(4):445–55. http://dx.doi.org/10.1080/15325008.2018.1449917.

[39] Lourenço LF, Monaro RM, Salles MB, Cardoso JR, Quéval L. Evaluation of the reactive power support capability and associated technical costs of photovoltaic farms' operation. Energies 2018;11(6). http://dx.doi.org/10.3390/en11061567.

[40] Alcahuaman H, Lopez JC, Dotta D, Rider MJ, Ghiocel S. Optimized reactive power capability of wind power plants with tap-changing transformers. IEEE Trans Sustain Energy 2021;12(4):1935–46. http://dx.doi.org/10.1109/TSTE.2021.3073658.

[41] Zhang B, Hou P, Hu W, Soltani M, Chen C, Chen Z. A reactive power dispatch strategy with loss minimization for a DFIG-based wind farm. IEEE Trans Sustain Energy 2016;7(3):914–23. http://dx.doi.org/10.1109/TSTE.2015.2509647, URL http://www.ieee.org/publications_standards/publications/rights/index.html.

[42] Ullah NR, Bhattacharya K, Thiringer T. Wind farms as reactive power ancillary service providers-technical and economic issues. IEEE Trans Energy Convers 2009;24(3):661–72. http://dx.doi.org/10.1109/TEC.2008.2008957.

[43] Kalambe S, Agnihotri G. Loss minimization techniques used in distribution network: Bibliographical survey. Renew Sustain Energy Rev 2014;29:184–200. http://dx.doi.org/10.1016/j.rser.2013.08.075.

[44] Usman M, Coppo M, Bignucolo F, Turri R. Losses management strategies in active distribution networks: A review. In: Electric power systems research. Vol. 163, Padova: Elsevier; 2018, p. 116–32. http://dx.doi.org/10.1016/j.epsr.2018.06.005.

[45] Ismael SM, Abdel Aleem SH, Abdelaziz AY, Zobaa AF. State-of-the-art of hosting capacity in modern power systems with distributed generation. In: Renewable energy. 2019, http://dx.doi.org/10.1016/j.renene.2018.07.008.

[46] Karthikeyan N. Hierarchical distributed control of active electric power distribution grids hierarchical distributed control of active electric power distribution grids by (Ph.D. thesis), 2019.

[47] Jabr RA. Optimal power flow using an extended conic quadratic formulation. IEEE Trans Power Syst 2008;23(3):1000–8. http://dx.doi.org/10.1109/TPWRS.2008.926439.

[48] Lavaei J, Low SH. Zero duality gap in optimal power flow problem. IEEE Trans Power Syst 2012;27(1):92–107. http://dx.doi.org/10.1109/TPWRS.2011.2160974.

[49] Jabr RA. Exploiting sparsity in SDP relaxations of the OPF problem. IEEE Trans Power Syst 2012;27(2):1138–9. http://dx.doi.org/10.1109/TPWRS.2011.2170772.

[50] Molzahn DK, Holzer JT, Lesieutre BC, DeMarco CL. Implementation of a large-scale optimal power flow solver based on semidefinite programming. IEEE Trans Power Syst 2013;28(4):3987–98. http://dx.doi.org/10.1109/TPWRS.2013.2258044.

[51] Low SH. Convex relaxation of optimal power flow - Part I Formulations and equivalence. IEEE Trans Control Netw Syst 2014;1(1):15–27. http://dx.doi.org/10.1109/TCNS.2014.2309732.

[52] Low SH. Convex relaxation of optimal power flow-part II: Exactness. IEEE Trans Control Netw Syst 2014;1(2):177–89. http://dx.doi.org/10.1109/TCNS.2014.2323634.

[53] Zhu H, Giannakis GB. Power system nonlinear state estimation using distributed semidefinite programming. IEEE J Sel Top Sign Proces 2014;8(6):1039–50. http://dx.doi.org/10.1109/JSTSP.2014.2331033.

[54] Yao Y, Liu X, Zhao D, Li Z. Distribution system state estimation: A semidefinite programming approach. IEEE Trans Smart Grid 2019;10(4):4369–78. http://dx.doi.org/10.1109/TSG.2018.2858140.

[55] Venzke A, Chatzivasileiadis S. Convex relaxations of security constrained AC optimal power flow under uncertainty. In: 20th power systems computation conference, PSCC 2018. Power Systems Computation Conference; 2018, http://dx.doi.org/10.23919/PSCC.2018.8442940.

[56] Davoodi E, Babaei E, Mohammadi-Ivatloo B, Shafie-Khah M, Catalao JP. Multiobjective optimal power flow using a semidefinite programming-based model. IEEE Syst J 2021;15(1):158–69. http://dx.doi.org/10.1109/JSYST.2020.2971838.

[57] Lavaei J. Zero duality gap for classical opf problem convexifies fundamental nonlinear power problems. In: Proceedings of the American control conference. Institute of Electrical and Electronics Engineers Inc.; 2011, p. 4566–73. http://dx.doi.org/10.1109/ACC.2011.5991104.

[58] Muljadi E, Butterfield CP, Ellis A, Mechenbier J, Hochheimer J, Young R, et al. Equivalencing the collector system of a large wind power plant preprint equivalencing the collector system of a large wind power plant. 2006.

[59] Muljadi E, Pasupulati S, Ellis A, Kosterov D. Method of equivalencing for a large wind power plant with multiple turbine representation. In: IEEE power and energy society 2008 general meeting: Conversion and delivery of electrical energy in the 21st century, PES. 2008, http://dx.doi.org/10.1109/PES.2008.4596055.

[60] Energi D. Guide for connection of power generating plants to the medium and high voltage grid above 1kV Type B, C, D. (April). 2019.

[61] Technical University of Denmark. Sophia HPC cluster. 2019, http://dx.doi.org/10.57940/fafc-6m81, URL https://dtu-sophia.github.io/docs/.

[62] Baviskar A, Hansen AD, Das K, Koivisto M. DTU 7k-bus active distribution network. In: Dataset. 2021, http://dx.doi.org/10.11583/DTU.c.5389910.v1.

[63] Baviskar A, Das K, Hansen AD. Minimize distribution network losses using wind power. CIRED - Open Access Proc J 2021;(September20-23):1–5.

[64] Statistics Denmark, [Online]. URL https://www.statbank.dk.